Symmetry-protected localized states at defects in non-Hermitian systems

Ya-Jie Wu[1,2,*] and Junpeng Hou[2,†]
[1]*School of Science, Xi'an Technological University, Xi'an 710032, China*
[2]*Department of Physics, The University of Texas at Dallas, Richardson, Texas 75080-3021, USA*

(Received 9 April 2019; published 12 June 2019)

Understanding how local potentials affect system eigenmodes is crucial for experimental studies of nontrivial bulk topology. Recent studies have discovered many exotic and highly nontrivial topological states in non-Hermitian systems. As such, it would be interesting to see how non-Hermitian systems respond to local perturbations. In this work we consider chiral and particle-hole-symmetric non-Hermitian systems on a bipartite lattice, including the Su-Schrieer-Heeger model and photonic graphene, and find that a disordered local potential could induce bound states evolving from the bulk. When the local potential on a single site becomes infinite, which renders a lattice vacancy, chiral-symmetry-protected zero-energy mode and particle-hole-symmetry-protected bound states with purely imaginary eigenvalues emerge near the vacancy. These modes are robust against any symmetry-preserved perturbations. Our work generalizes the symmetry-protected localized states to non-Hermitian systems.

DOI: 10.1103/PhysRevA.99.062107

I. INTRODUCTION AND MOTIVATION

A non-Hermitian Hamiltonian captures the essentials of open systems governed by non-Hermitian operators [1–10], for instance, optical and mechanical structures with gain and loss [11–23]. Intriguingly, although non-Hermitian operators usually have complex eigenvalues, the energy spectra of a non-Hermitian Hamiltonian with parity-time ($\mathcal{PT}$) symmetry could be real valued in $\mathcal{PT}$-symmetric regimes. Such a reality could also be broken by tuning, for example, the gain or loss strength, and in the resultant $\mathcal{PT}$-broken regime, the $\mathcal{PT}$ symmetry is said to be broken spontaneously [24,25]. $\mathcal{PT}$-symmetry breaking has already been observed in optical waveguides [26]. Similar physics exists in $\mathcal{CP}$ symmetry, where $\mathcal{C}$ denotes particle-hole symmetry, due to the antilinearity of $\mathcal{C}$ and $\mathcal{T}$. For a $\mathcal{CP}$-symmetric Hamiltonian H, $\mathcal{CP}$ and $\mathcal{PT}$ symmetries are equivalent under the transformation $H \to iH$ [27–29]. Consequently, the eigenenergies of a $\mathcal{CP}$-symmetric system is imaginary when $\mathcal{CP}$ symmetry is preserved in the spectrum. Otherwise, it could be real in the $\mathcal{CP}$-broken regimes.

In contrast, topological states have attracted intensive attention in various Hermitian systems [30,31]. Recently, the concept of topological phases has been extended to non-Hermitian systems. $\mathcal{C}$ and $\mathcal{T}$ symmetries are unified by non-Hermiticity, which allows topological phases in high dimensions. The interplay between topology and non-Hermiticity leads to rich topological features with no Hermitian counterpart [32–46]. In particular, the conventional bulk-boundary correspondence breaks down in non-Hermitian systems and new topological invariants like the non-Bloch topological invariant and vorticity must be introduced to understand the underlying topological properties.

The nontrivial bulk topology in Hermitian systems can be detected by defects such as edges, π flux, dislocations, and vortices [47–52]. When it comes to non-Hermitian systems, stable edge states could also exist at the interface between topological and trivial phases [28,53–60]. These topological states, originated from bulk topologies, are immune to local symmetry-preserved perturbations. It is well known that a local potential could induce localized modes in topological phases of Hermitian systems [61–63], while such a problem has been far less investigated in non-Hermitian systems. In addition, recent studies of topological states in open systems have found many novel and unique topological phases in non-Hermitian systems. In this sense, it is worth investigating how a local potential affects the system eigenmodes in non-Hermitian systems. In general, for a bipartite lattice with a Hamiltonian H obeying the symmetry $\mathcal{O}H\mathcal{O}^{-1} = -H$, the quantum states are paired with opposite real parts of eigenvalues. Then, once a single lattice site is removed by an infinite local potential, an unpaired mode with zero or purely imaginary energy appears.

In this work we generalize the idea to non-Hermitian systems and show the robustness of the induced bound states. Specifically, we focus on both one-dimensional (1D) and 2D systems with two sublattice degrees of freedoms, respecting either chiral ($\mathcal{O} = \mathcal{S}$) or particle-hole ($\mathcal{O} = \mathcal{C}$) symmetry, which are responsible for versatile symmetry-protected topological phases in low dimensions. We show that, in the cases of non-Hermitian systems, the lattice vacancy can induce symmetry-protected localized modes in both topological and trivial phases.

The rest of this paper is organized as follows. In Sec. II we discuss $\mathcal{S}$ and $\mathcal{C}$ symmetries on a bipartite lattice and derive the eigenvalue-correspondence relation. We start with a 1D system in Sec. III, namely, the non-Hermitian

*wuyajie@xatu.edu.cn
†junpeng.hou@utdallas.edu

Su-Schrieffer-Heeger (SSH) model with either $\mathcal{S}$ or $\mathcal{C}$ symmetry, and study the effects of a lattice vacancy. In Sec. IV we extend the study to 2D photonic graphene. We apply both symmetry analysis and numerical calculations to investigate how lattice vacancies change the system eigenmodes. Conclusions and a discussion are presented in Sec. V.

II. CHIRAL AND PARTICLE-HOLE SYMMETRIES IN NON-HERMITIAN SYSTEMS

In this section we study the general theory of symmetry-protected modes induced by vacancies. For simplicity, we consider non-Hermitian effective models on a bipartite lattice (sublattices A and B). In momentum space, the generic effective Hamiltonian is $\hat{H} = \sum_k \Psi_k^\dagger H(k) \Psi_k$, with $\hat{\Psi}_k^\dagger = (\hat{a}_k^\dagger, \hat{b}_k^\dagger)$ and

$$H(k) = \boldsymbol{h}_0 \cdot \boldsymbol{\sigma} + i\boldsymbol{h}_1 \cdot \boldsymbol{\sigma}, \tag{1}$$

where σ_0 and $\boldsymbol{\sigma} = (\sigma_x, \sigma_y, \sigma_z)$ are an identity matrix and Pauli matrices that act on sublattice space, respectively, and $\boldsymbol{h}_i = (h_{i,x}, h_{i,y}, h_{i,z})$, $i = 0, 1$, are real.

First, we consider $\mathcal{S}$ symmetry described by $\mathcal{S}H(k)\mathcal{S}^{-1} = -H(k)$, where S is a unitary operator. When $S = \sigma_z$ is chosen in this basis, we obtain

$$H(k) = h_{0,x}\sigma_x + h_{0,y}\sigma_y + ih_{1,x}\sigma_x + ih_{1,y}\sigma_y. \tag{2}$$

If ψ_k is an eigenstate for the Hamiltonian $H(k)$ with eigenvalue E_k, $\mathcal{S}\psi_k$ is an eigenstate for the Hamiltonian $H(k)$ with eigenvalue $-E_k$. Thus, for the above non-Hermitian system on a bipartite lattice, there exists the energy-eigenvalue correspondence $E_k \Leftrightarrow -E_k$. This symmetry dictates that energy eigenvalues must be paired.

Second, let us consider $\mathcal{C}$ symmetry described by $\mathcal{C}H(k)\mathcal{C}^{-1} = -H(-k)$ and $\mathcal{C}$ symmetry being antiunitary.[1] When $\mathcal{C} = \sigma_z K$ is chosen in this basis, we have

$$H(k) = h_{0,x}\sigma_x + h_{0,y}\sigma_y + ih_{1,z}\sigma_z, \tag{3}$$

with the constraints $h_{0,x}(k) = h_{0,x}(-k)$, $h_{0,y}(k) = -h_{0,y}(-k)$, and $h_{1,z}(k) = h_{1,z}(-k)$. Provided ψ_k is an eigenstate with eigenvalue E_k for the Hamiltonian $H(k)$, $\mathcal{C}\psi_k$ is an eigenstate of the Hamiltonian $H(-k)$ with eigenvalue $-E_k^*$. Therefore, the energy spectrum has the correspondence $E_k \Leftrightarrow -E_{-k}^*$ under periodic boundary conditions. This symmetry classifies energy eigenvalues in complex-conjugate pairs, except when they are purely imaginary.

Consider an $\mathcal{S}$-symmetric non-Hermitian system with N_u unit cells. If a lattice site is removed (corresponds to a lattice vacancy defect), the translational symmetry is broken, but the $\mathcal{S}$ symmetry of the Hamiltonian is still preserved through the transformations $\hat{a}_i \Rightarrow \hat{a}_i$, $\hat{b}_i \Rightarrow -\hat{b}_i$, and $\hat{H} \Rightarrow -\hat{H}$, where $\hat{a}_i$ ($\hat{b}_i$) denotes annihilation operators on lattice site i of sublattice A (B). Now, only $2N_\mathrm{u} - 1$ quantum states are available, which leads to the energy-eigenvalue correspondence $E_{1,\ldots,N_\mathrm{u}-1} \Leftrightarrow -E_{N_\mathrm{u}+1,\ldots,2N_\mathrm{u}-1}$, i.e., only $2N_\mathrm{u} - 2$ states are paired. To guarantee $\mathcal{S}$ symmetry, the single left unpaired state must satisfy $E_{N_\mathrm{u}} \Leftrightarrow -E_{N_\mathrm{u}}$, which means that the remaining single state must have zero eigenenergy. While this argument is the same for Hermitian and non-Hermitian systems, the physics is richer with non-Hermiticity, as we will see later.

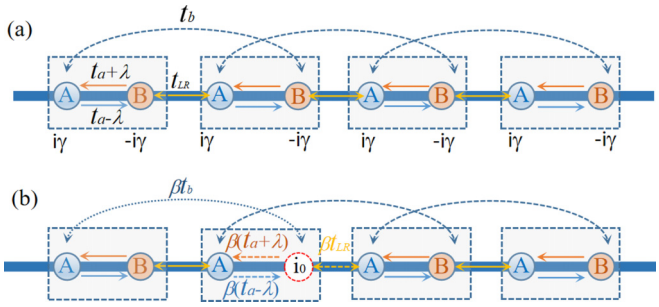

FIG. 1. Illustration of the non-Hermitian SSH model. The dotted rectangle denotes the unit cell. (a) Here $t_a \pm \lambda$, t_{LR}, and t_b are tunneling strengths and $\pm i\gamma$ denote balanced gain and loss. (b) The red dashed circle at i_0 denotes the site under a local potential $V_d = V_0(1-\beta)/\beta$. The hopping amplitude related to this site is proportional to β.

Next we consider a $\mathcal{C}$-symmetric non-Hermitian system with N_u unit cells. When a single lattice site is removed, a lattice vacancy arises and $2N_\mathrm{u} - 1$ quantum states remain. At this time, the $\mathcal{C}$ symmetry of the system is also respected through the particle-hole transformation $\hat{a}_i \Rightarrow \hat{a}_i^\dagger$, $\hat{b}_i \Rightarrow -\hat{b}_i^\dagger$, and $\hat{H} \Rightarrow -\hat{H}$, which leads to the energy-eigenvalue correspondence $E_{1,\ldots,N_\mathrm{u}-1} \Leftrightarrow -E^*_{N_\mathrm{u}+1,\ldots,2N_\mathrm{u}-1}$, i.e., $2N_\mathrm{u} - 2$ states are conjugate paired. To guarantee C symmetry, the single left unpaired state must satisfy $E_{N_\mathrm{u}} \Leftrightarrow -E^*_{N_\mathrm{u}}$, which means that this single unpaired state has either zero or purely imaginary energy. Obviously, the latter is only feasible in non-Hermitian systems.

In the following, we will provide two concrete examples to elucidate both $\mathcal{S}$- and $\mathcal{C}$-symmetry-protected modes induced by a lattice vacancy.

III. SU-SCHRIEFFER-HEEGER MODEL

In this section we consider the non-Hermitian SSH model shown in Fig. 1(a), which is relevant to the current experiments. The generic Bloch Hamiltonian is

$$H_{S,0}(k) = h_{0,x}\sigma_x + (h_{0,y} + i\lambda)\sigma_y + i\gamma\sigma_z, \tag{4}$$

where $h_{0,x} = t_a + (t_{LR} + t_b)\cos k$ and $h_{0,y} = (t_{LR} - t_b)\sin k$. Note that $i\lambda\sigma_y$ and $i\gamma\sigma_z$ are non-Hermitian parameters, which stem from unequal hopping strength within a unit cell and balanced gain and loss, respectively. Hereafter, we will discuss chiral- and particle-hole-symmetry-protected modes induced by the lattice vacancy.

A. Chiral-symmetry-protected mode

When $\gamma = 0$, the model has a chiral symmetry $\sigma_z H_{S,0}(k)\sigma_z^{-1} = -H_{S,0}(k)$. It has been studied in Ref. [42],

[1] We remark that in a rigorous classification of symmetry classes of non-Hermitian systems, the particle-hole symmetry is unitary, contrary to its Hermitian counterpart. However, since the full classification has not been achieved yet, we still call the $\mathcal{C}$ symmetry particle-hole symmetry in this work, following most of the current literature.

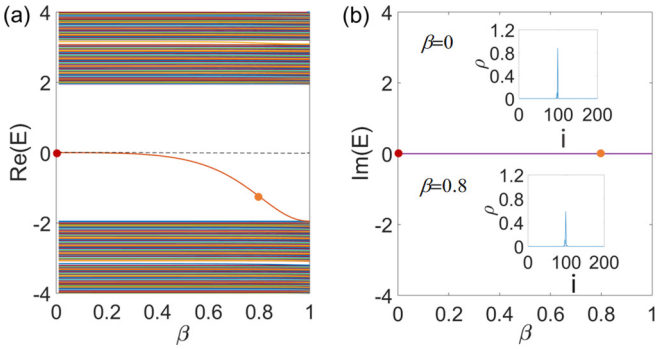

FIG. 2. Spectrum of the SSH model with respect to varying disordered strength β, showing the (a) real and (b) imaginary parts of the eigenvalues. The top (bottom) inset shows the particle-density distribution of localized mode with $\beta = 0$ ($\beta = 0.8$) in real space. The parameters are $t_a = 1.5$, $\lambda = 0.1$, $t_{LR} = 1.0$, $t_b = 0.1$, $\gamma = 0$, $V_0 = 10.0$, and $N_u = 100$.

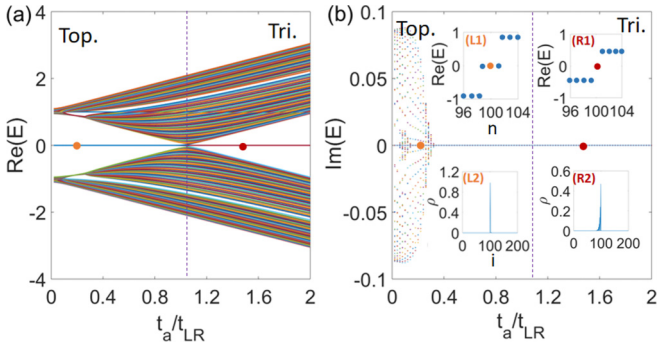

FIG. 3. (a) Real and (b) imaginary spectra of the SSH model with chiral symmetry. The orange and red dots indicate two zero-energy states localized near the vacancy in two topologically distinct phases. The insets (L1) and (L2) in (b) show the real part of energies $\mathrm{Re}(E)$ versus the indices of states n and the particle density distribution ρ versus lattice site indices i of the vacancy-induced zero-energy mode in the topological phase (Top.) [$\beta = 0.2$, indicated by the orange dot in (a) and (b)], respectively. The insets (R1) and (R2) present $\mathrm{Re}(E)$ and ρ of the zero-energy mode in trivial phase (Tri.) [$\beta = 1.5$, indicated by the red dot in (a) and (b)], respectively. The parameters are $\lambda = 0.1$, $t_{LR} = 1.0$, $t_b = 0.1$, $\gamma = 0$, $V_0 = 10.0$, and $N_u = 100$.

where the issue of the breakdown of conventional bulk-boundary correspondence has been settled and non-Bloch bulk-boundary correspondence was introduced. Chiral symmetry ensures that the eigenvalues appear in $(E_k, -E_k)$ pairs. If a vacancy exists [see Fig. 1(b)], the translational symmetry is broken. However, the chiral symmetry is still respected by the Hamiltonian. Because the SSH model is based on a bipartite lattice, an unpaired state exists. Due to the eigenvalue-correspondence relation discussed in the preceding section, the leftover state must have exactly zero energy.

Next we numerically study the effects of a lattice vacancy on the quantum states within the system. The vacancy can be seen as a hole in the system by removing a lattice site. To simulate the vacancy, we gradually vary the local potential on a given site i_0 labeled in Fig. 1(b). The overall Hamiltonian is then $\hat{H}_{S,0} = \hat{H}_{S,0}(i \neq i_0) + \hat{H}_V$, where $\hat{H}_{S,0}(i \neq i_0)$ does not contain terms related to the site i_0, and $\hat{H}_V$ is

$$\hat{H}_V = \beta \sum_{i_0,j} \left(t_{i_0,j} \hat{c}^\dagger_{i_0} \hat{c}_j + t_{j,i_0} \hat{c}^\dagger_j \hat{c}_{i_0} \right) + \sum_{i_0} V_d \hat{c}^\dagger_{i_0} \hat{c}_{i_0}. \quad (5)$$

Here $t_{i_0,j}$ (t_{j,i_0}) denotes the bare hopping amplitude (without local disordered potential) between sites j and i_0 and the local potential reads $V_d = V_0(1-\beta)/\beta$. When $\beta = 1$, the local potential $V_d = 0$. The Hamiltonian $\hat{H}_V$ reduces to $\hat{H}_0$ and exhibits translational invariance. As β decreases, V_d gradually increases. When $\beta \to 0$, the local potential $V_d \to \infty$ and the effective hopping amplitude related to site i_0 approaches zero. This corresponds to a lattice vacancy at site i_0. The numerical results are shown in Fig. 2. We see that all eigenvalues are real. As β decreases, the wave function evolves from an extended state to an in-gap state. For $0 < \beta < 1$, chiral symmetry is observed to be broken in the spectra by a bound state. Such a localized state resides in the energy gap, which is labeled by the solid tangerine curve in Fig. 2(a). When β approaches zero, an exact zero-energy state exists and the energy spectrum becomes symmetric. The insets of Fig. 2(b) showcase the particle-density distribution of localized modes in real space.

It is known that there is a topological phase transition by tuning t_a/t_{LR} [42], but the chiral symmetry is always respected. To see how the vacancy-induced zero-energy modes respond to topological phase transitions, we choose an open-boundary chain ($2N_u$ lattice sites with a single vacancy) and calculate the eigenvalues at different t_a/t_{LR}. The numerical results are shown in Fig. 3. There are two distinct phases, i.e., the topological phase and the trivial phase. In the topological phase, besides the two edge states, there is another zero-energy state localized near the vacancy, as shown in insets (L1) and (L2) of Fig. 3(b). In the trivial phase, the edge states disappear, but the state localized near the vacancy survives, as shown in insets (R1) and (R2) of Fig. 3(b). The wave function could be spatially extended as t_b increases, but its energy always remains zero. In summary, such a chiral-symmetric zero-energy bound state is robust to topological phase transition.

B. Particle-hole-symmetry-protected mode

When $\lambda = 0$, the model has particle symmetry, which ensures that the eigenvalues appear in $(E_k, -E_k^*)$ pairs. In addition, this model also has $\mathcal{PT}$ symmetry $\sigma_x H^*_{S,0}(k)\sigma_x = H_{S,0}(-k)$; consequently, it may possess a real spectrum. However, $\mathcal{PT}$ symmetry could be spontaneously broken in the interval $t_a - \gamma < t_{LR} < t_a + \gamma$, leaving complex energies in the spectrum [56]. We apply the same methods to simulate the vacancy and study its effects on the system. The Hamiltonian is $\hat{H} = \hat{H}_{S,0}(i \neq i_0) + \hat{H}_V$, where $\hat{H}_V$ is the same as Eq. (5) except that $V_d = i\epsilon_{i_0}\gamma/\beta$ with $\epsilon_{i_0 \in A} = +1$ and $\epsilon_{i_0 \in B} = -1$. Obviously, if $\beta = 1$, the system reduces the Hamiltonian $\hat{H}_{S,0}$ and exhibits translational symmetry. As β decreases, the amplitude for V_d increases, but the hopping amplitude related to the site i_0 decreases. As $\beta \to 0$, the effective hopping amplitude from or to the site i_0 approaches zero and $|V_d|$

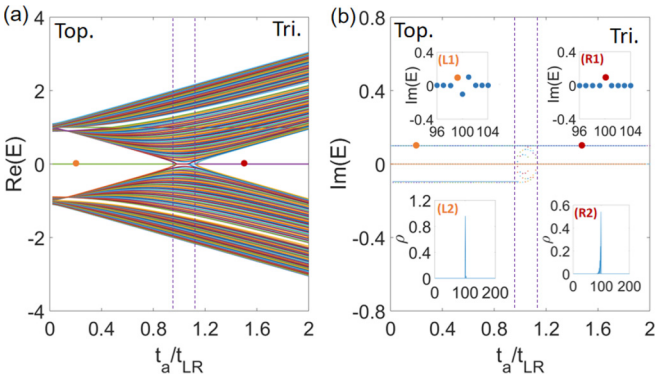

FIG. 4. Similar to Fig. 3 but plotted with different non-Hermitian parameters $\lambda = 0$ and $\gamma = 0.1$.

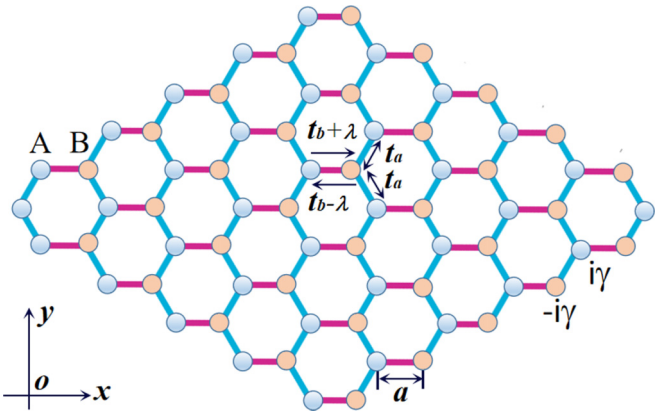

FIG. 5. Illustration of a honeycomb lattice. The parameters t_a and $t_b \pm \lambda$ are tunneling strengths and $\pm i\gamma$ denote balanced gain and loss. The lattice spacing is set as $a = 1$.

becomes infinite. When $\beta = 0$, a lattice vacancy appears at site i_0.

Let us numerically study the system with a single vacancy ($\beta = 0$), of which the translational symmetry is broken, but the particle-hole symmetry is still respected. Because the SSH model is based on a bipartite lattice, an unpaired state exists. Due to the spectral symmetry ($E \leftrightarrow -E^*$), the unpaired state must have exactly zero or purely imaginary energy. We calculate eigenenergies for a chain with a single vacancy under open boundary conditions. The numerical results are shown in Fig. 4 and there are two distinct phases. In the topological phase, there are two edge states with imaginary energies $\pm i\gamma$, as verified in Fig. 4. In the presence of a lattice vacancy, in both phases a state with purely imaginary energy $+i\gamma$ ($-i\gamma$) is localized near the vacancy if $i_0 \in B$ (A), as shown in the energy distribution in the insets (L1) and (R1) of Fig. 4(b). In the topological phase, when the vacancy site $i_0 \in B$, because of $t_a < t_{LR}$, the localized state extends to the B site on the right, as confirmed by the density distribution in the inset (L2) of Fig. 4(b). In contrast, in the trivial phase, due to $t_a > t_{LR}$, the localized state extends to the B site on the left, as shown in the inset (R2) of Fig. 4(b). If $i_0 \in A$, the extension direction of the localized state is opposite to that when $i_0 \in B$. Due to the particle-hole symmetry, the unpaired bound state with $E = \pm i\gamma$ cannot acquire a finite real energy through any perturbations with $\mathcal{C}$ symmetry, but may only change its imaginary part. This robust pinning to zero real energy is protected by $\mathcal{C}$ symmetry. Here we also would like to remark that the vacancy-induced localized states are robust to $\mathcal{PT}$-symmetry breaking, as they are to the topological phase transition (see Appendix A for more details).

IV. PHOTONIC GRAPHENE

In this section we consider the 2D honeycomb lattice sketched in Fig. 5, which is relevant to photonic graphenes [60,64–71]. The Bloch Hamiltonian on the honeycomb lattice reads $H_{G,0}(k) = h_{0,x}\sigma_x + (h_{0,y} + i\lambda)\sigma_y + i\gamma\sigma_z$, where $h_{0,x} = t_b + 2t_a \cos(3k_x/2)\cos(\sqrt{3}k_y/2)$ and $h_{0,y} = -2t_a \sin(3k_x/2)\cos(\sqrt{3}k_y/2)$. Uneven hopping amplitudes introduce the non-Hermitian term $i\lambda\sigma_y$, and the balanced gain and loss give rise to $i\gamma\sigma_z$. In the absence of non-Hermitian terms, i.e., $\lambda = \gamma = 0$, this corresponds to isotropic graphene if $t_a/t_b = 1$. As $|t_a/t_b|$ decreases, C_3 symmetry is broken and the two Dirac nodes of vorticity $\pm\pi$ gradually approach each other and finally meet up and are annihilated at a time-reversal invariant momentum at $|t_a/t_b| = 1/2$. As $|t_a/t_b|$ decreases further, the system enters a gapped topological phase, dubbed a high-order topological insulator, which hosts zero-energy corner modes [72,73]. In the presence of a non-Hermitian term $i\lambda\sigma_y$ or $i\gamma\sigma_z$, the corner modes remain as shown in Figs. 6 and 7; this will be detailed in the following.

A. Chiral-symmetry-protected modes

In the absence of gain and loss, i.e., $\gamma = 0$, this system has chiral symmetry. The zero-energy corner modes localize at the corner. In addition, the chiral symmetry ensures that the eigenvalues appear in $(E_k, -E_k)$ pairs. Similar to the analysis for the SSH model in the preceding section, we introduce a disordered local potential on one site. By gradually varying the local potential as in Sec. III A, a bound state also evolves from the bulk states and localizes near the defect. We

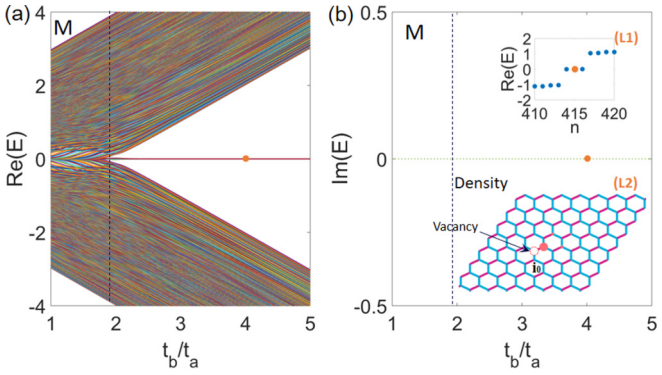

FIG. 6. (a) Real and (b) complex spectra of the graphene model with chiral symmetry versus the parameter t_b/t_a. The orange disk indicates the zero-energy state localized near the vacancy in the gapped phase. The top inset (L1) shows the real part of energies when $t_b/t_a = 4.0$ and the bottom inset (L2) shows the density distribution of the localized zero mode. The density is proportional to the radius of the pink spots. The parameters are $\lambda = 0.2$, $t_a = 1.0$, and $\gamma = 0$.

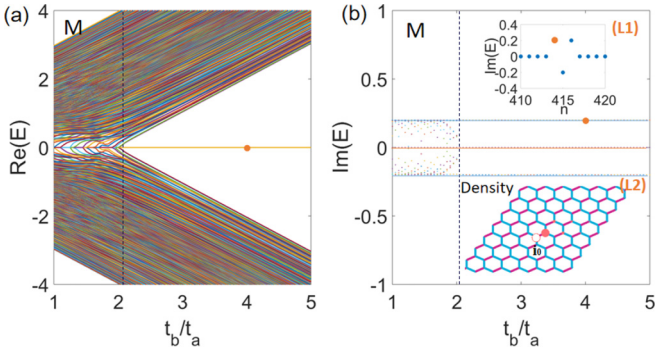

FIG. 7. Similar to Fig. 6 but with modified non-Hermitian parameters $\lambda = 0$ and $\gamma = 0.2$.

numerically compute the quantum states of this honeycomb lattice model (32×26 lattice) with vacancy site i_0 under open boundary conditions. Figures 6(a) and 6(b) present the real and imaginary parts of energies of the states, respectively. There are two distinct phases, namely, the metallic phase (M) and the gapped phase. In addition to the two zero-energy corner modes, we find that a localized zero mode [solid orange dot in (L1) of Fig. 6] appears near the vacancy, as shown in the inset (L2).

B. Particle-hole-symmetry-protected modes

If $\lambda = 0$, the particle-hole symmetry is respected. Because of the eigenvalue correspondence ($E \leftrightarrow -E^*$), the unpaired state must have exactly zero energy or a purely imaginary energy. We repeat the numerical processes and the results are plotted in Fig. 7. In the gapped phase, there are two corner states with imaginary energies $\pm i\gamma$. The lattice vacancy induces an extra state (indicated by the orange disk) with purely imaginary energy $+i\gamma$ ($-i\gamma$) localized near the vacancy if $i_0 \in B$ (A). In the gapped phase, when the vacancy site is located at $i_0 \in A$, because $t_a < t_b$, the localized state extends to the B site on the right, which is verified by numerics in the bottom inset (L2) of Fig. 7(b). However, if $i_0 \in A$, the extension direction would be the opposite, similar to the non-Hermitian SSH model.

V. DISCUSSION AND CONCLUSION

In the presence of multivacancies, there exists a parity effect, which states that for a system with an odd number of vacancies, there always exists a symmetry-protected mode due to the eigenvalue correspondence, while for a system with an even number of vacancies, the localized states would possess a finite-energy shift due to quantum tunneling effects. A numeric investigation of this matter is discussed in Appendix B. In this paper we mainly study one- and two-dimensional systems. The general theory is also applicable to three-dimensional lattice systems, such as the diamond lattice model. In fact, the obtained result is applicable not only for the bipartite-lattice models, but also for the lattice models with a unit cell of an even number of sites preserving chiral or particle-hole symmetry [74]. These conclusions can also be generalized to Hermitian systems with chiral or particle-hole symmetry, where the zero mode gives rise to a fractional charge [75]. The non-Hermitian SSH model and graphene model may be realized by optical lattices, and the vacancy-induced localized modes could be detected with current experimental techniques.

In summary, we have studied the vacancy-induced localized modes in non-Hermitian systems with either chiral or particle-hole symmetries. The localized states are symmetry protected in the sense they are robust against perturbations respecting the underlying symmetries.

ACKNOWLEDGMENTS

This work was supported by NSFC through Grant No. 11504285, the Scientific Research Program Funded by Natural Science Basic Research Plan in Shaanxi Province of China (Programs No. 2018JQ1058 and No. 2019JM-001), the Scientific Research Program Funded by Shaanxi Provincial Education Department through Grant No. 18JK0397, and a scholarship from China Scholarship Council (Program No. 201708615072).

APPENDIX A: ROBUSTNESS TO $\mathcal{PT}$-SYMMETRY BREAKING

Generally, the exceptional point is crucial for understanding many important physical phenomena in non-Hermitian systems and it happens when the system experiences a spontaneous symmetry breaking. In the main text, we focus on the symmetry-protected modes induced by local potentials at fixed on-site gain or loss strength. To illustrate the role of $\mathcal{PT}$-symmetry breaking and exceptional points, we study the spectrum through varying the gain or loss strength γ, as shown in Fig. 8, which shows that the system undergoes a $\mathcal{PT}$-symmetry breaking at the exceptional point γ_c, where the bulk spectrum turns from real to imaginary. However, we find that any nonzero γ would render a localized mode with purely imaginary energy, as indicated by the red line in Fig. 8, due to the particle-hole symmetry. So the vacancy-induced localized states are robust to $\mathcal{PT}$-symmetry breaking, as they are to the topological phase transition.

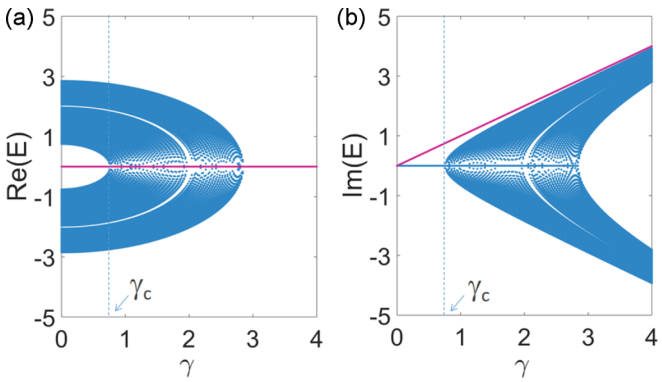

FIG. 8. (a) Real part Re(E) and (b) imaginary part Im(E) of the eigenenergies of the SSH model with a single lattice vacancy versus the gain or loss strength γ. The other parameters are fixed as $t_a = 1.8$, $t_{LR} = 1$, $t_b = 0.1$, and $\lambda = 0$.

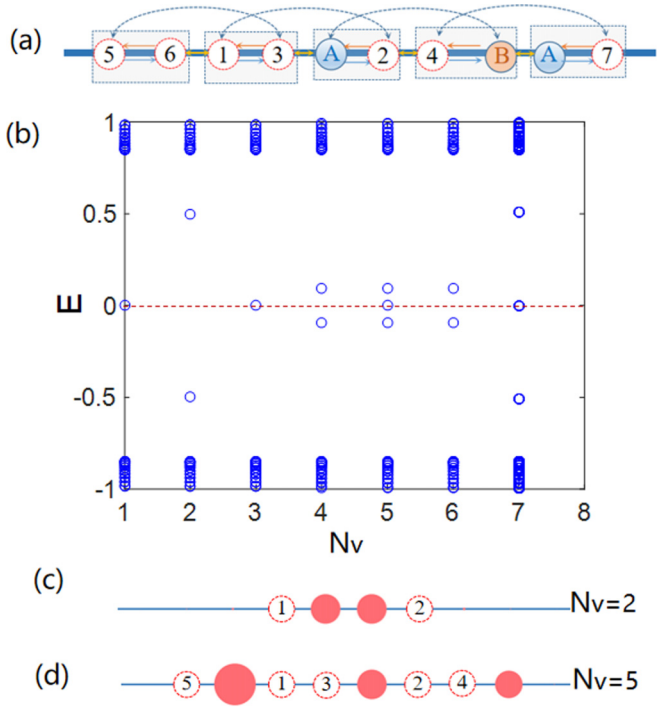

FIG. 9. (a) The SSH model with multivacancies. (b) Eigenenergies of the SSH model versus the the number of vacancies. Here $N_v = m$ corresponds to vacancies existing at sites $1, 2, \ldots, m$, as shown in (a). Also shown is the particle density distribution of localized modes in the presence of (c) $N_v = 2$ and (d) $N_v = 5$ vacancies. The density is proportional to the radius of the pink spots. The parameters are $t_a = 1.4$, $t_{LR} = 0.5$, $t_b = 0.1$, $\lambda = 0.1$, $\gamma = 0$, and $N_u = 100$.

APPENDIX B: PARITY EFFECT IN THE PRESENCE OF MULTIVACANCIES

Without loss of generality, we take the chiral symmetric SSH as an example to illustrate the parity effect regarding multivacancies. In the presence of multivacancies, as illustrated in Fig. 9(a), the symmetry-protected localized mode exhibits a parity effect.

First, in the presence of an odd number of vacancies ($N_v = 1, 3, 5, 7$), there always exists a localized zero-energy mode guaranteed by the chiral symmetry, as confirmed by Fig. 9(b). Figure 9(d) showcases the particle density distribution of localized modes with an odd number ($N_v = 5$) of vacancies in real space. Besides the zero-energy localized mode (indicated by the bigger pink spot), there are also two localized in-gap modes with finite energy (indicated by the two smaller pink spots, less localized than the zero-energy mode). Second, for the system with an even number of vacancies, the tunneling effect could give rise to an energy splitting, so the zero-energy state may disappear. For instance, the case of $N_v = 2$ demonstrates this point, as shown in Fig. 9(b). However, the in-gap modes possessing finite energy may also be localized near vacancies, as shown in Fig. 9(c) in the case of an even number ($N_v = 2$) of vacancies.

In particle-hole symmetric non-Hermitian systems with multivacancies, the parity effect also exists in analogy to that in the aforementioned chiral symmetric systems. The particle-hole-symmetry-protected localized mode with zero or purely imaginary energy always exists in the presence of an odd number of vacancies, while for a system with an even number of vacancies, the localized states would possess a finite-energy shift due to tunneling effects.

[1] H. J. Carmichael, Phys. Rev. Lett. **70**, 2273 (1993).
[2] I. Rotter, J. Phys. A: Math. Theor. **42**, 153001 (2009).
[3] Y. Choi, S. Kang, S. Lim, W. Kim, J.-R. Kim, J.-H. Lee, and K. An, Phys. Rev. Lett. **104**, 153601 (2010).
[4] S. Diehl, E. Rico, M. A. Baranov, and P. Zoller, Nat. Phys. **7**, 971 (2011).
[5] T. E. Lee and C.-K. Chan, Phys. Rev. X **4**, 041001 (2014).
[6] T. E. Lee, F. Reiter, and N. Moiseyev, Phys. Rev. Lett. **113**, 250401 (2014).
[7] S. Malzard, C. Poli, and H. Schomerus, Phys. Rev. Lett. **115**, 200402 (2015).
[8] B. Zhen, C. W. Hsu, Y. Igarashi, L. Lu, I. Kaminer, A. Pick, S.-L. Chua, J. D. Joannopoulos, and M. Soljačić, Nature (London) **525**, 354 (2015).
[9] H. Cao and J. Wiersig, Rev. Mod. Phys. **87**, 61 (2015).
[10] P. San-Jose, J. Cayao, E. Prada, and R. Aguado, Sci. Rep. **6**, 21427 (2016).
[11] K. G. Makris, R. El-Ganainy, D. N. Christodoulides, and Z. H. Musslimani, Phys. Rev. Lett. **100**, 103904 (2008).
[12] Y. D. Chong, L. Ge, and A. D. Stone, Phys. Rev. Lett. **106**, 093902 (2011).
[13] A. Regensburger, C. Bersch, M. A. Miri, G. Onishchukov, D. N. Christodoulides, and U. Peschel, Nature (London) **488**, 167 (2012).
[14] H. Hodaei, M. A. Miri, M. Heinrich, D. N. Christodoulides, and M. Khajavikhan, Science **346**, 975 (2014).
[15] B. Peng, Ş. K. Özdemir, S. Rotter, H. Yilmaz, M. Liertzer, F. Monifi, C. M. Bender, F. Nori, and L. Yang, Science **346**, 328 (2014).
[16] L. Feng, Z. J. Wong, R. M. Ma, Y. Wang, and X. Zhang, Science **346**, 972 (2014).
[17] H. Jing, S. K. Özdemir, X. Y. Lü, J. Zhang, L. Yang, and F. Nori, Phys. Rev. Lett. **113**, 053604 (2014).
[18] B. Peng, Ş. K. Özdemir, F. Lei, F. Monifi, M. Gianfreda, G. L. Long, S. Fan, F. Nori, C. M. Bender, and L. Yang, Nat. Phys. **10**, 394 (2014).
[19] Z. P. Liu, J. Zhang, Ş. K. Özdemir, B. Peng, H. Jing, X. Y. Lü, C. W. Li, L. Yang, F. Nori, and Y. X. Liu, Phys. Rev. Lett. **117**, 110802 (2016).
[20] K. Kawabata, Y. Ashida, and M. Ueda, Phys. Rev. Lett. **119**, 190401 (2017).
[21] Y. Ashida, S. Furukawa, and M. Ueda, Nat. Commun. **8**, 15791 (2017).
[22] S. Weimann, M. Kremer, Y. Plotnik, Y. Lumer, S. Nolte, K. G. Makris, M. Segev, M. C. Rechtsman, and A. Szameit, Nat. Mater. **16**, 433 (2017).
[23] R. El-Ganainy, K. G. Makris, M. Khajavikhan, Z. H. Musslimani, S. Rotter, and D. N. Christodoulides, Nat. Phys. **14**, 11 (2018).

[24] C. M. Bender and S. Boettcher, Phys. Rev. Lett. **80**, 5243 (1998).
[25] C. M. Bender, Rep. Prog. Phys. **70**, 947 (2007).
[26] C. E. Rüter, K. G. Makris, R. El-Ganainy, D. N. Christodoulides, M. Segev, and D. Kip, Nat. Phys. **6**, 192 (2010).
[27] K. Kawabata, S. Higashikawa, Z. Gong, Y. Ashida, and M. Ueda, Nat. Commun. **10**, 297 (2019).
[28] R. Okugawa and T. Yokoyama, Phys. Rev. B **99**, 041202(R) (2019).
[29] K. Yamamoto, M. Nakagawa, K. Adachi, K. Takasan, M. Ueda, and N. Kawakami, arXiv:1903.04720.
[30] M. Z. Hasan and C. L. Kane, Rev. Mod. Phys. **82**, 3045 (2010).
[31] X.-L. Qi and S.-C. Zhang, Rev. Mod. Phys. **83**, 1057 (2011).
[32] M. S. Rudner and L. S. Levitov, Phys. Rev. Lett. **102**, 065703 (2009).
[33] S.-D. Liang and G.-Y. Huang, Phys. Rev. A **87**, 012118 (2013).
[34] B. Zhu, R. Lü, and S. Chen, Phys. Rev. A **89**, 062102 (2014).
[35] D. Leykam, K. Y. Bliokh, C. Huang, Y. D. Chong, and F. Nori, Phys. Rev. Lett. **118**, 040401 (2017).
[36] Z. Gong, S. Higashikawa, and M. Ueda, Phys. Rev. Lett. **118**, 200401 (2017).
[37] J. González and R. A. Molina, Phys. Rev. B **96**, 045437 (2017).
[38] H. Shen, B. Zhen, and L. Fu, Phys. Rev. Lett. **120**, 146402 (2018).
[39] S. Lieu, Phys. Rev. B **97**, 045106 (2018).
[40] C. Yin, H. Jiang, L. Li, R. Lü, and S. Chen, Phys. Rev. A **97**, 052115 (2018).
[41] C. Li, X. Z. Zhang, G. Zhang, and Z. Song, Phys. Rev. B **97**, 115436 (2018).
[42] S. Yao and Z. Wang, Phys. Rev. Lett. **121**, 086803 (2018).
[43] S. Yao, F. Song, and Z. Wang, Phys. Rev. Lett. **121**, 136802 (2018).
[44] Z. Gong, Y. Ashida, K. Kawabata, K. Takasan, S. Higashikawa, and M. Ueda, Phys. Rev. X **8**, 031079 (2018).
[45] K. Kawabata, Y. Ashida, H. Katsura, and M. Ueda, Phy. Rev. B **98**, 085116 (2018).
[46] G. Harari, M. A. Bandres, Y. Lumer, M. C. Rechtsman, Y. D. Chong, M. Khajavikhan, D. N. Christodoulides, and M. Segev, Science **359**, eaar4003 (2018).
[47] C. Weeks, G. Rosenberg, B. Seradjeh, and M. Franz, Nat. Phys. **3**, 796 (2007).
[48] S. Tewari, S. Das Sarma, and D.-H. Lee, Phys. Rev. Lett. **99**, 037001 (2007).
[49] G. Rosenberg, B. Seradjeh, C. Weeks, and M. Franz, Phys. Rev. B **79**, 205102 (2009).
[50] R. Roy, Phys. Rev. Lett. **105**, 186401 (2010).
[51] L. Santos, Y. Nishida, C. Chamon, and C. Mudry, Phys. Rev. B **83**, 104522 (2011).
[52] V. Juricic, A. Mesaros, R. J. Slager, and J. Zaanen, Phys. Rev. Lett. **108**, 106403 (2012).
[53] C. Yuce, Phys. Rev. A **93**, 062130 (2016).
[54] C. Yuce, Phys. Rev. A **98**, 012111 (2018).
[55] L.-J. Lang, Y. Wang, H. Wang, and Y. D. Chong, Phys. Rev. B **98**, 094307 (2018).
[56] C. Yuce, Phys. Rev. A **97**, 042118 (2018).
[57] J. C. Budich, J. Carlstrom, F. K. Kunst, and E. J. Bergholtz, Phys. Rev. B **99**, 041406(R) (2019).
[58] T. Yoshida, R. Peters, N. Kawakami, and Y. Hatsugai, Phys. Rev. B **99**, 121101(R) (2019).
[59] H. Zhou, J. Yeon Lee, S. Liu, and B. Zhen, Optica **6**, 190 (2019).
[60] Z. Oztas and C. Yuce, Phys. Rev. A **98**, 042104 (2018).
[61] W. Y. Shan, J. Lu, H. Z. Lu, and S. Q. Shen, Phys. Rev. B **84**, 035307 (2011).
[62] A. V. Balatsky, I. Vekhter, and J. X. Zhu, Rev. Mod. Phys. **78**, 373 (2006).
[63] J. Lu, W. Y. Shan, H. Z. Lu, and S. Q. Shen, New J. Phys. **13**, 103016 (2011).
[64] Y. Plotnik, M. C. Rechtsman, D. Song, M. Heinrich, J. M. Zeuner, S. Nolte, Y. Lumer, N. Malkova, J. Xu, A. Szameit, Z. Chen, and M. Segev, Nat. Mater. **13**, 57 (2014).
[65] N. K. Efremidis, S. Sears, D. N. Christodoulides, J. W. Fleischer, and M. Segev, Phys. Rev. E **66**, 046602 (2002).
[66] O. Peleg, G. Bartal, B. Freedman, O. Manela, M. Segev, and D. N. Christodoulides, Phys. Rev. Lett. **98**, 103901 (2007).
[67] R. A. Sepkhanov, Y. B. Bazaliy, and C. W. J. Beenakker, Phys. Rev. A **75**, 063813 (2007).
[68] O. Bahat-Treidel, O. Peleg, and M. Segev, Opt. Lett. **33**, 2251 (2008).
[69] G. Bartal, O. Cohen, H. Buljan, J. W. Fleischer, O. Manela, and M. Segev, Phys. Rev. Lett. **94**, 163902 (2005).
[70] M. Polini, F. Guinea, M. Lewenstein, H. C. Manoharan, and V. Pellegrini, Nat. Nanotech. **8**, 625 (2013).
[71] O. Bahat-Treidel, O. Peleg, M. Grobman, N. Shapira, M. Segev, and T. Pereg-Barnea, Phys. Rev. Lett. **104**, 063901 (2010).
[72] M. Ezawa, Phys. Rev. B **99**, 121411(R) (2019).
[73] M. Ezawa, Phys. Rev. B **98**, 045125 (2018).
[74] W. A. Benalcazar, B. A. Bernevig, and T. L. Hughes, Science **357**, 61 (2017).
[75] J. He, Y.-X. Zhu, Y.-J. Wu, L.-F. Liu, Y. Liang, and S.-P. Kou, Phys. Rev. B **87**, 075126 (2013).